

2009

# Spectroscopic study of the benchmark $Mn^{+}-H_2$ complex

Viktoras Dryza  
*University Of Melbourne*

Berwyck L. J Poad  
*University of Wollongong, bpoad@uow.edu.au*

Evan J. Bieske  
*University Of Melbourne*

---

## Publication Details

Dryza, V., Poad, B. L. J. & Bieske, E. J. (2009). Spectroscopic study of the benchmark  $Mn^{+}-H_2$  complex. *Journal of Physical Chemistry A*, 113 (21), 6044-6048.

---

# Spectroscopic study of the benchmark $Mn^+-H_2$ complex

## Abstract

We have recorded the rotationally resolved infrared spectrum of the weakly bound  $Mn^+-H_2$  complex in the H-H stretch region (4022-4078  $cm^{-1}$ ) by monitoring  $Mn^+$  photodissociation products. The band center of  $Mn^+-H_2$ , the H-H stretch transition, is shifted by -111.8  $cm^{-1}$  from the transition of the free  $H_2$  molecule. The spectroscopic data suggest that the  $Mn^+-H_2$  complex consists of a slightly perturbed  $H_2$  molecule attached to the  $Mn^+$  ion in a T-shaped configuration with a vibrationally averaged intermolecular separation of 2.73 Å. Together with the measured  $Mn^+...H_2$  binding energy of 7.9 kJ/mol (Weis, P.; et al. *J. Phys. Chem. A* 1997, 101, 2809.), the spectroscopic parameters establish  $Mn^+-H_2$  as the most thoroughly characterized transition-metal cation-dihydrogen complex and a benchmark for calibrating quantum chemical calculations on noncovalent systems involving open d-shell configurations. Such systems are of possible importance for hydrogen storage applications.

## Keywords

spectroscopic,  $h_2$ , complex, study, benchmark, mn, GeoQUEST

## Disciplines

Life Sciences | Physical Sciences and Mathematics | Social and Behavioral Sciences

## Publication Details

Dryza, V., Poad, B. L. J. & Bieske, E. J. (2009). Spectroscopic study of the benchmark  $Mn^+-H_2$  complex. *Journal of Physical Chemistry A*, 113 (21), 6044-6048.

## ARTICLES

Spectroscopic Study of the Benchmark  $\text{Mn}^+-\text{H}_2$  Complex

Viktoras Dryza, Berwyck L. J. Poad, and Evan J. Bieske\*

School of Chemistry, The University of Melbourne, Victoria, Australia 3010

Received: April 6, 2009

We have recorded the rotationally resolved infrared spectrum of the weakly bound  $\text{Mn}^+-\text{H}_2$  complex in the H–H stretch region (4022–4078  $\text{cm}^{-1}$ ) by monitoring  $\text{Mn}^+$  photodissociation products. The band center of  $\text{Mn}^+-\text{H}_2$ , the H–H stretch transition, is shifted by  $-111.8 \text{ cm}^{-1}$  from the transition of the free  $\text{H}_2$  molecule. The spectroscopic data suggest that the  $\text{Mn}^+-\text{H}_2$  complex consists of a slightly perturbed  $\text{H}_2$  molecule attached to the  $\text{Mn}^+$  ion in a T-shaped configuration with a vibrationally averaged intermolecular separation of 2.73 Å. Together with the measured  $\text{Mn}^+\cdots\text{H}_2$  binding energy of 7.9 kJ/mol (Weis, P.; et al. *J. Phys. Chem. A* 1997, 101, 2809.), the spectroscopic parameters establish  $\text{Mn}^+-\text{H}_2$  as the most thoroughly characterized transition-metal cation–dihydrogen complex and a benchmark for calibrating quantum chemical calculations on noncovalent systems involving open d-shell configurations. Such systems are of possible importance for hydrogen storage applications.

## 1. Introduction

Whereas hydrogen is an attractive candidate as a clean fuel for transport purposes, it has proved difficult to develop appropriate technologies for its efficient, safe, and economical storage.<sup>1,2</sup> Materials that bind intact dihydrogen molecules through weak physisorption interactions ( $\sim 10$ – $50 \text{ kJ/mol}$ ) are attractive storage candidates because they are able to absorb and release  $\text{H}_2$  rapidly and reversibly at low temperatures. Several materials containing transition-metal atoms have been suggested for this purpose. For example, transition-metal atoms integrated into carbon nanostructures are predicted to coordinate multiple dihydrogen molecules with electron donation from the metal atoms to the carbon nanostructure enhancing binding because of electrostatic interactions.<sup>3–7</sup> Metal–organic frameworks (MOF), microporous network materials consisting of metal atoms connected by bridging organic molecules, constitute another class of materials that can store hydrogen through physisorption. MOFs with exposed transition-metal atom sites are particularly promising because direct dihydrogen interactions at these oxidized sites are stronger than those at shielded sites.<sup>8</sup> Information on the interaction between the  $\text{H}_2$  and the exposed metal atom has been obtained through infrared (IR) spectroscopy<sup>9,10</sup> and neutron scattering,<sup>11–13</sup> although the low thermal stability of some MOFs renders the latter technique almost unusable.<sup>8</sup>

Here we present a gas-phase spectroscopic study of the manganese cation–dihydrogen complex ( $\text{Mn}^+-\text{H}_2$ ), a small, fundamental system that is appropriate for understanding the interaction between dihydrogen and a transition-metal cation. The rotationally resolved IR spectrum of  $\text{Mn}^+-\text{H}_2$  is obtained in the H–H stretch region, with the analysis yielding accurate vibrational frequencies and structural parameters that are related to the strength of the metal-cation–dihydrogen bond. Although IR spectra for noncovalent molecular complexes containing

open-shell transition-metal cations have previously been reported,<sup>14,15</sup> spectra exhibiting resolved rovibrational features, which allow bond distances to be extracted, are rare.

The spectroscopic data for  $\text{Mn}^+-\text{H}_2$  can be used to gauge the efficacy of different computational approaches currently used to understand the  $\text{H}_2$  interaction with metal atoms in carbon nanostructures and MOFs and to guide the rational development of new materials.<sup>3–7,10,16–18</sup> Computational exploration of the transition-metal atoms' role in hydrogen storage materials is usually performed using density functional theory (DFT). For reasonably large systems, the results obtained are similar to those from ab initio methods, yet they require substantially less computing time. Nonetheless, systems containing a transition-metal atom are challenging subjects for DFT because of the number of electrons and bonding orbitals. Usually, effective core potentials and smaller d-orbital basis sets are employed to make the calculations viable (albeit less precise). DFT can also have difficulties in calculating the properties of systems with partially filled d-orbital configurations, with the results depending on which exchange and correlation functionals are implemented.<sup>19</sup> Moreover, DFT does not account for dispersion forces, which can play an important role in weak physisorption interactions.<sup>20</sup>

Before performing quantum chemical calculations on realistic hydrogen storage systems, the chosen computational method should preferably be calibrated using a smaller subsystem such as  $\text{Mn}^+-\text{H}_2$  for which there are accurate experimental data, thereby engendering confidence in the computational approach and helping identify systematic errors.

Interactions between  $\text{H}_2$  and the first-row transition-metal cations ( $\text{M}^+$ ) have previously been explored experimentally through measurements of gas-phase clustering equilibria and theoretically through DFT calculations. (See ref 21 and references contained within.) As shown for  $\text{Mn}^+-\text{H}_2$  in Figure 1, the  $\text{M}^+-\text{H}_2$  complexes are predicted to have T-shaped structures, a configuration favored by the electrostatic charge–

\* Corresponding author. E-mail: evanjeb@unimelb.edu.au.

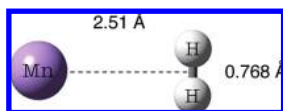


**Figure 1.** Calculated structure for  $\text{Mn}^+-\text{H}_2$  taken from ref 22.

quadrupole interaction and by electron donor–acceptor bonding. The interaction between  $\text{H}_2$  and  $\text{Mn}^+$  in its  $^7\text{S}$  ground electronic state (a  $4s^13d^5$  configuration) is particularly weak ( $D_0 \approx 7.9$  kJ/mol) because of Pauli repulsion between electrons in the large, singly occupied  $\text{Mn}^+$   $4s$  orbital and the filled  $\text{H}_2$   $1\sigma$  orbital.<sup>22</sup> Although promotion of the  $4s$  electron to give a  $3d^6$  configuration would reduce this repulsion, the resulting  $^5\text{D}$  state lies substantially higher in energy (1.82 eV).<sup>23</sup> In fact, the repulsion is ameliorated to some extent by partial hybridization of the  $4s$  orbital with the higher energy  $4p_z$  orbital, resulting in transfer of electron density away from the intermolecular region. Back bonding from the  $\text{Mn}^+$   $d_{yz}$   $\pi$  orbital into the  $\text{H}_2$   $2\sigma^*$  antibonding orbital does not contribute to the interaction because back donation from a half-filled  $d$   $\pi$  orbital reduces  $d$ – $d$  exchange stabilization energy.<sup>22,24</sup>

The weak nature of the  $\text{Mn}^+\cdots\text{H}_2$  bond is evident from the structural parameters calculated using the B3LYP method and a split valence plus polarization (SVP) function basis set,<sup>22</sup> which predict an intermolecular bond length of 2.51 Å and an increase in the H–H bond length compared with the free  $\text{H}_2$  molecule of only 0.002 Å. (See Figure 1.)

## 2. Experimental and Computational Approach

Conveniently, the weak intermolecular bond makes  $\text{Mn}^+-\text{H}_2$  a suitable candidate for interrogation using IR photodissociation spectroscopy. This experimental approach relies on absorption of a single IR photon by the  $\text{H}_2$  subunit with the deposited vibrational energy migrating into the weak intermolecular bond, which subsequently ruptures. Because the H–H stretch ( $\nu_{\text{HH}}$ ) frequency of  $\text{Mn}^+-\text{H}_2$  is only slightly reduced compared with the free  $\text{H}_2$  molecule ( $4161\text{ cm}^{-1}$ ), excitation of this vibrational mode is sufficient to sever the weak  $\text{Mn}^+\cdots\text{H}_2$  bond ( $D_0 \approx 660\text{ cm}^{-1}$ ).<sup>22</sup>

The IR photodissociation experiments were conducted using a home-built tandem mass spectrometer that has been used for studies of other similar  $\text{M}^+-\text{H}_2$  complexes ( $\text{M} = \text{Li}, \text{B}, \text{Na}, \text{Mg},$  and  $\text{Al}$ ).<sup>25–30</sup> Briefly, the  $\text{Mn}^+-\text{H}_2$  complexes were generated by laser vaporization of a 4 mm diameter manganese rod adjacent to a supersonic expansion of pure  $\text{H}_2$  gas. The central portion of the supersonic expansion was selected by a skimmer and passed into a quadrupole mass filter that was tuned to the mass of  $\text{Mn}^+-\text{H}_2$ . Next, the  $\text{Mn}^+-\text{H}_2$  ions were turned  $90^\circ$  by an electrostatic bender into an octapole ion guide where they were overlapped with a counterpropagating IR beam originating from an optical parametric oscillator (Continuum Mirage 3000,  $0.017\text{ cm}^{-1}$  bandwidth). The IR beam could be tuned over the  $4000$ – $4200\text{ cm}^{-1}$  range corresponding to the  $\nu_{\text{HH}}$  region of the  $\text{H}_2$  subunit. IR light that was resonant with a rovibrational  $\nu_{\text{HH}}$  transition of  $\text{Mn}^+-\text{H}_2$  caused the complex to break up into  $\text{Mn}^+$  and  $\text{H}_2$  fragments. A second quadrupole mass filter selected any resulting  $\text{Mn}^+$  fragments, which passed to an ion detector. We obtained the IR spectrum by monitoring the  $\text{Mn}^+$  photofragment intensity as a function of IR wavelength.

Complementary DFT calculations were performed using the Gaussian 03 computational software to determine the optimized geometry, binding energy, and harmonic vibrational frequencies of the  $\text{Mn}^+-\text{H}_2$  complex.<sup>31</sup> For this investigation, the two hybrid DFT methods B3LYP and PBE1PBE were utilized. Ahlrich's

triple- $\zeta$  valence plus polarization (TZVP) all-electron basis set was used for both the Mn and H atoms. Pure spherical harmonic functions were used with this basis set, and the calculations were performed on a large grid of size (99, 590). The purpose of the present computational investigation is to determine how well the  $\text{Mn}^+-\text{H}_2$  complex is described by DFT methods with basis sets commonly applied to investigate larger hydrogen storage systems. Although ab initio calculations with very large basis sets are computationally viable on small systems such as  $\text{Mn}^+-\text{H}_2$ , they are currently not feasible for larger model systems used to replicate hydrogen storage materials.

For each DFT method, the calculated  $\nu_{\text{HH}}$  frequency of  $\text{Mn}^+-\text{H}_2$  was scaled by the factor required to reconcile the calculated  $\nu_{\text{HH}}$  frequency of the free  $\text{H}_2$  molecule with the experimental value (scaling factor of 0.9405 for B3LYP/TZVP and 0.9418 for PBE1PBE/TZVP). The  $\nu_{\text{HH}}$  frequency of  $\text{Mn}^+-\text{H}_2$  calculated by Bowers and coworkers<sup>22</sup> was adjusted in a similar way (scaling factor 0.9533). Corrections to the calculated binding energies due to zero-point energies and basis set superposition effects were included.

## 3. Results and Discussion

**3.1. Analysis of the Infrared Spectrum.** The  $\text{Mn}^+-\text{H}_2$  complex is anticipated to be a near-prolate asymmetric rotor because the moments of inertia about the  $B$  and  $C$  axes are almost equal and are much larger than the moment of inertia about the  $A$  axis (i.e., the intermolecular axis).<sup>22</sup> Excitation of the  $\nu_{\text{HH}}$  mode causes a dipole moment change along the intermolecular axis, resulting in rovibrational transitions that are characteristic of a parallel A-type band. The transition selection rules are  $\Delta K_a = 0$  and  $\Delta K_c = \pm 1$ , where  $K_a$  and  $K_c$  are the projections of the rotational angular momentum ( $\hat{N}$ ) along the  $A$  and  $C$  axes, respectively. The selection rules for the rotational angular momentum are  $\Delta N = 0, \pm 1$  ( $\Delta N = \pm 1$ ) for the  $K_a > 0$  ( $K_a = 0$ ) states. The rotational angular momentum ( $\hat{N}$ ) and electronic spin ( $\hat{S}$ ) are related to the total angular momentum (excluding nuclear spin) by  $\hat{J} = \hat{N} + \hat{S}$ . Transition selection rules for the total angular momentum excluding nuclear spin are  $\Delta J = 0, \pm 1$  ( $\Delta J = \pm 1$ ) for the  $K_a > 0$  ( $K_a = 0$ ) states. Although each  $N$  level is associated with  $7J$  sublevels, the spectral structure associated with spin-rotation splitting is not resolved in this study so that the observed transitions can be assigned in terms of  $N$ ,  $K_a$ , and  $K_c$ .

The  $\text{Mn}^+-\text{H}_2$  IR spectrum in the  $4022$ – $4078\text{ cm}^{-1}$   $\nu_{\text{HH}}$  region (Figure 2) displays full rotational resolution and has an appearance that is compatible with the predicted T-shaped  $\text{C}_{2v}$  structure of the complex (Figure 1). Only  $K_a = 1-1$  sub-band transitions, associated with complexes containing the ortho modification of  $\text{H}_2$ , have significant intensity. The predominance of complexes containing the ortho form (i.e., odd  $K_a$ ) over those containing the para form (i.e., even  $K_a$ ) is expected; as for normal  $\text{H}_2$  gas, the ortho/para ratio is 3:1. Furthermore,  $\text{Mn}^+-\text{H}_2$  (para) complexes are rapidly converted to the more stable  $\text{Mn}^+-\text{H}_2$  (ortho) complexes through exothermic ligand switching reactions in the ion source.<sup>27,32</sup>

The  $K_a = 1-1$  sub-band displays a P branch ( $\Delta N = -1$ ), Q branch ( $\Delta N = 0$ ), and R branch ( $\Delta N = +1$ ), as labeled in Figure 2. The peaks in the P and R branches appear as doublets because of asymmetry splitting (i.e.,  $\Delta K_c = \pm 1$ ). Each peak of the doublet should consist of seven overlapping subcomponent transitions corresponding to the different possible values of  $J$  for each value of  $N$ . Although these subcomponent transitions are unresolved, they may contribute to the widths of the observed lines (fwhm  $\approx 0.07\text{ cm}^{-1}$ ). Other possible contributions

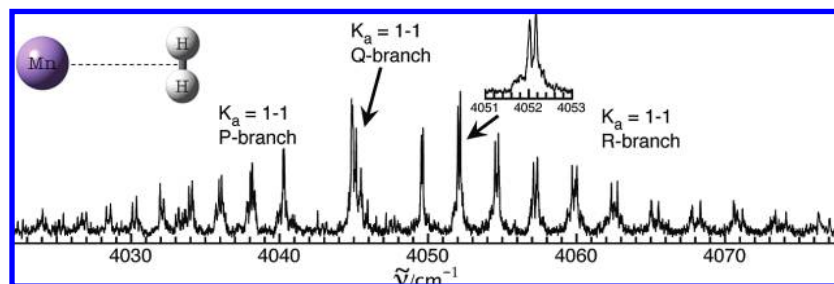


**Figure 2.** Infrared spectrum of  $\text{Mn}^+-\text{H}_2$  in the H–H stretch region obtained by monitoring  $\text{Mn}^+$  photofragments. The P, Q, and R branches of the  $K_a = 1-1$  sub-band are labeled.

**TABLE 1: Spectroscopic Constants for  $\text{Mn}^+-\text{H}_2$  Derived by Fitting the  $\nu_{\text{HH}} K_a = 1-1$  Transitions to a Watson A-Reduced Hamiltonian<sup>a</sup>**

	exptl		calcd		
	$n_{\text{HH}} = 0$	$n_{\text{HH}} = 1$	B3LYP/SVP <sup>b</sup>	B3LYP/TZVP <sup>c</sup>	PBE1PBE/TZVP <sup>d</sup>
$B$	1.1752(12)	1.2082(12)			
$C$	1.1296(12)	1.1597(12)			
$\bar{B}$	1.1524(12)	1.1839(12)			
$\Delta_J \times 10^4$	1.48(10)	1.36(10)			
$\nu_{\text{sub}}^e$	4044.85(1)				
$\nu_{\text{HH}}^f$	4049.4(1.5)		4059	4037	4036
$\Delta\nu_{\text{HH}}^f$	-111.8(1.5)		-102	-124	-125
$R/\text{\AA}^g$	2.73	2.69	2.51	2.57	2.56
$\omega_s$	203	221	320	296	299
$\omega_b$			391	369	391
$D_0^h$	660(140)		890	538	570

<sup>a</sup> Unless otherwise indicated, units are  $\text{cm}^{-1}$ . For each value, the error in the last significant figure(s) is given in parentheses. Calculated DFT values are also given. <sup>b</sup> Calculated values from ref 22. <sup>c</sup> B3LYP with Ahlrich's triple- $\zeta$  valence plus polarization (TZVP) all-electron basis. <sup>d</sup> PBE1PBE with Ahlrich's triple- $\zeta$  valence plus polarization (TZVP) all-electron basis. <sup>e</sup> Sub-band origin for  $K_a = 1-1$  transitions. <sup>f</sup> DFT  $\nu_{\text{HH}}$  and  $\Delta\nu_{\text{HH}}$  values are scaled by the factors required to reconcile calculated and measured  $\text{H}_2$  stretch frequencies. (See the text.) <sup>g</sup> Experimental data are vibrationally averaged separations ( $R_0$ ), whereas calculated values are equilibrium separations ( $R_e$ ). <sup>h</sup> Experimental  $D_0$  from ref 22.

to the line-widths include lifetime broadening of the excited vibrational state due to coupling with the  $\text{Mn}^+ + \text{H}_2$  dissociation continuum, power broadening, and a  $0.017 \text{ cm}^{-1}$  contribution from the IR bandwidth.

The  $K_a = 1-1$  sub-band transitions were fitted to an A-reduced Watson Hamiltonian yielding the spectroscopic parameters presented in Table 1. The ground- and excited-state A rotational constants cannot be determined from a parallel A-type band because the fits  $A''$  and  $A'$  were constrained to the rotational constant of the free  $\text{H}_2$  molecule in the ground vibrational state ( $B'' = 59.33 \text{ cm}^{-1}$ ).<sup>33</sup> The  $\nu_{\text{HH}}$  band center is expected to lie between  $\Delta B$  and  $2\Delta B$  higher in energy than the  $K_a = 1-1$  sub-band center ( $4044.9 \text{ cm}^{-1}$ ), where  $\Delta B = B'' - B' \approx 3 \text{ cm}^{-1}$  is the difference between the rotational constant of the free  $\text{H}_2$  molecule in its ground and excited vibrational states.<sup>33</sup> The two limits are based on the  $\text{Mn}^+-\text{H}_2$  complex being either a rigid T-shaped rotor or, alternatively, exhibiting free internal rotation of the  $\text{H}_2$  subunit. Because the actual situation will lie between these two extremes, the  $\nu_{\text{HH}}$  band center is deemed to be the average of the two limits, that is,  $4049.4 \pm 1.5 \text{ cm}^{-1}$ . This implies that the transition is displaced by  $-111.8 \text{ cm}^{-1}$  from the  $Q_1(0)$  transition of the free  $\text{H}_2$  molecule ( $4161.2 \text{ cm}^{-1}$ ).<sup>33</sup>

The vibrationally averaged intermolecular  $\text{Mn}^+\cdots\text{H}_2$  separation estimated from  $\bar{B} = (B + C)/2$  is  $2.73 \text{ \AA}$ , contracting by

$0.04 \text{ \AA}$  upon vibrational excitation of the  $\text{H}_2$  subunit. The contraction is presumably due to an increase in the vibrationally averaged polarizability and quadrupole moment of the  $\text{H}_2$  molecule leading to an enhancement of the electrostatic and induction interactions.<sup>34</sup> The equilibrium  $\text{Mn}^+\cdots\text{H}_2$  separation is not immediately derivable from the vibrationally averaged intermolecular separation. However, comparisons with  $\text{Na}^+-\text{H}_2$ , which has a binding energy and intermolecular bond length similar to those of  $\text{Mn}^+-\text{H}_2$ , and for which an accurate potential energy surface has been constructed and used to calculate rovibrational energy levels suggest that the equilibrium separation should be around  $0.1 \text{ \AA}$  less than the vibrationally averaged value (i.e.,  $\sim 2.63 \text{ \AA}$ ).<sup>28</sup>

Because of the weak intermolecular bond and large rotational constant of the  $\text{H}_2$  subunit, the  $\text{Mn}^+-\text{H}_2$  complex is expected to exhibit considerable zero-point motion in the bending vibration coordinate. This floppiness is manifested in an exaggerated difference between the  $B$  and  $C$  constants compared with a rigid T-shaped structure.<sup>35</sup> Consequently the inertial defect  $1/C - 1/B - 1/A$  is not zero (as it would be for a rigid planar molecule) so that the  $A$  constant and the H–H bond distance cannot be determined from  $B$  and  $C$ .

**3.2. Density Functional Theory Calculations.** In this section, we briefly compare the measured properties of  $\text{Mn}^+-\text{H}_2$  with the results of previous B3LYP/SVP and current B3LYP/TZVP and PBE1PBE/TZVP DFT calculations, with particular reference to the dissociation energy, the intermolecular separation, the harmonic intermolecular stretching frequency, and the stretching frequency of the  $\text{H}_2$  subunit.

At the outset, it is worthwhile to recall that  $\text{Mn}^+-\text{H}_2$  is a weakly bound complex that exhibits large-amplitude, zero-point excursions in the intermolecular stretch and bend vibrational coordinates (even when the complex is in its ground vibrational state). There are several consequences of this floppiness. First, the intermolecular vibrational modes will probably have frequencies lower than the DFT harmonic estimates. Therefore, the calculated dissociation energy,  $D_0$ , estimated using a zero-point energy calculated from the harmonic vibrational frequencies, will tend to underestimate the actual binding energy. Second, because of zero-point vibrational excursions (particularly in the  $R$  coordinate), the calculated intermolecular separation,  $R_e$ , is likely to be less than the vibrationally averaged separation,  $R_0$ , deduced from the rotational constants. Third, because of stretch–bend coupling, the harmonic stretching frequency estimated from the rotational and centrifugal distortion constants will probably be lower than the ab initio estimate (which is related to the second derivative of the potential energy along the  $R$  coordinate at the PES minimum). Even in the ground vibrational state, the complex undergoes large-amplitude bending excursions, sampling regions of the PES where the  $\text{Mn}^+\cdots\text{H}_2$  radial attraction is weaker than it is in the T-shaped



equilibrium configuration. This reduces the effective radial force constant, causing the experimental  $\omega_s$  value to be less than the DFT harmonic estimate.

Eventually, making full contact between experiment and theory requires the development of a 3D PES that is subsequently used to calculate the rovibrational energies of the complex. This procedure has not yet been accomplished for  $\text{Mn}^+-\text{H}_2$  but has been accomplished for the  $\text{Na}^+-\text{H}_2$  complex, which has a similar binding energy (660 and 860  $\text{cm}^{-1}$ , respectively).<sup>28</sup> Therefore, the findings for  $\text{Na}^+-\text{H}_2$  should provide a guide for  $\text{Mn}^+-\text{H}_2$ .

The experimental and DFT data for  $\text{Mn}^+-\text{H}_2$  are summarized in Table 1. From the experimental  $\bar{B}$  value, one can deduce a vibrationally averaged intermolecular separation ( $R_0 = 2.73 \text{ \AA}$ ) that is 0.22, 0.16, and 0.17  $\text{Å}$  greater than the equilibrium separations predicted, respectively, by the B3LYP/SVP, B3LYP/TZVP and PBE1PBE/TZVP levels. For  $\text{Na}^+-\text{H}_2$ , the vibrationally averaged separation,  $R_0$ , exceeds the equilibrium separation,  $R_e$ , by  $\sim 0.1 \text{ \AA}$ , and it seems likely that  $R_0$  exceeds  $R_e$  by a similar amount in  $\text{Mn}^+-\text{H}_2$ . This would imply that the B3LYP/TZVP and PBE1PBE/TZVP levels do a reasonable job of predicting the equilibrium intermolecular separation. The experimental  $\omega_s$  value (203  $\text{cm}^{-1}$ ) is around 30% lower than the DFT estimates (320, 296, and 299  $\text{cm}^{-1}$  for B3LYP/SVP, B3LYP/TZVP, and PBE1PBE/TZVP levels). A similar reduction ( $\sim 20\%$ ) for the experimental  $\omega_s$  value compared with the ab initio harmonic estimate was found for  $\text{Na}^+-\text{H}_2$  because of stretch–bend coupling.

The harmonic bending frequencies ( $\omega_b$ ) calculated using the B3LYP/SVP, B3LYP/TZVP and PBE1PBE/TZVP DFT levels (391, 369, and 391  $\text{cm}^{-1}$ , respectively) are comparable to the calculated barrier for internal rotation of the  $\text{H}_2$  subunit (402 and 453  $\text{cm}^{-1}$  at the B3LYP/TZVP and PBE1PBE/TZVP levels) and therefore obviously overestimate the actual bending frequency.

In general, the B3LYP/SVP, B3LYP/TZVP and PBE1PBE/TZVP DFT levels all do a reasonable job of estimating the experimental  $\nu_{\text{HH}}$  frequency (4049.4  $\text{cm}^{-1}$ ). One derives scaled frequencies of 4059, 4037, and 4036  $\text{cm}^{-1}$ , respectively, if the harmonic DFT frequencies are scaled by the appropriate factor so that the method reproduces the frequency of the bare  $\text{H}_2$  molecule.

As far as the binding energy is concerned, the experimental value ( $660 \pm 140 \text{ cm}^{-1}$ ) is underestimated by the B3LYP/TZVP and PBE1PBE/TZVP levels (538 and 570  $\text{cm}^{-1}$ , respectively) and overestimated by the B3LYP/SVP level (890  $\text{cm}^{-1}$ ). As explained above, because of an overestimation of the two intermolecular vibrational modes' frequencies, the DFT dissociation energy is likely to underestimate the actual value (as is the case for the B3LYP/TZVP and PBE1PBE/TZVP levels). Compared with  $\text{Na}^+-\text{H}_2$ , for which the difference is 8%, the discrepancy is larger for  $\text{Mn}^+-\text{H}_2$  (18 and 14% for the B3LYP/TZVP and PBE1PBE/TZVP levels), perhaps because  $\text{Mn}^+-\text{H}_2$  is more weakly bound than  $\text{Na}^+-\text{H}_2$  and the two intermolecular modes are more anharmonic.

In summary, the B3LYP/TZVP and PBE1PBE/TZVP levels appear to give reasonable descriptions of the  $\text{Mn}^+-\text{H}_2$  complex regarding the binding energy, the intermolecular bond length, and the intermolecular stretch frequency. The B3LYP/SVP level used by Bowers and coworkers overestimates the binding energy and may also underestimate the intermolecular separation slightly.

**3.3. Comparisons with Related Complexes.** The  $\Delta\nu_{\text{HH}}$  vibrational shift for ion complexes containing  $\text{H}_2$  is sometimes presumed to be linearly correlated with the binding energy

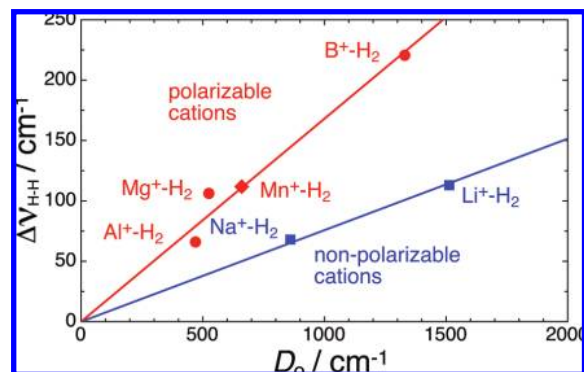


**Figure 3.** Frequency shift for the H–H stretch vibration ( $\Delta\nu_{\text{HH}}$ ) plotted against dissociation energy ( $D_0$ ) for  $\text{M}^+-\text{H}_2$  complexes ( $\text{M} = \text{Li}, \text{B}, \text{Na}, \text{Mg}, \text{Al},$  and  $\text{Mn}$ ). The plotted data are experimental values (from refs 22, 26–30 and 36–38) apart from the  $D_0$  values of  $\text{Li}^+-\text{H}_2$  and  $\text{Mg}^+-\text{H}_2$ , which are calculated values taken from refs 39 and 40, respectively.

( $D_0$ ).<sup>41,42</sup> Therefore, it is interesting to compare  $\Delta\nu_{\text{HH}}$  and  $D_0$  for  $\text{Mn}^+-\text{H}_2$  with corresponding values for the  $\text{Li}^+-\text{H}_2$ ,  $\text{B}^+-\text{H}_2$ ,  $\text{Na}^+-\text{H}_2$ ,  $\text{Mg}^+-\text{H}_2$ , and  $\text{Al}^+-\text{H}_2$  complexes that have also been studied spectroscopically,<sup>26–30</sup> theoretically,<sup>39,40</sup> and thermochemically.<sup>22,36–38</sup> In general, complexes containing the  $\text{Mn}^+$ ,  $\text{B}^+$ ,  $\text{Mg}^+$ , and  $\text{Al}^+$  cations, which have a singly or doubly occupied valence s orbital, exhibit a larger  $\Delta\nu_{\text{HH}}$  red shift for a given dissociation energy than complexes containing the  $\text{Li}^+$  and  $\text{Na}^+$  cations. The trends are apparent in Figure 3 where  $\Delta\nu_{\text{HH}}$  is plotted against  $D_0$ ; data for complexes containing cations with a half-filled or filled valence s orbital ( $\text{B}^+$ ,  $\text{Mg}^+$ ,  $\text{Al}^+$ , and  $\text{Mn}^+$ ) and data for complexes containing alkali metal cations ( $\text{Li}^+$ ,  $\text{Na}^+$ ) lie on separate lines. In general, the large  $\Delta\nu_{\text{HH}}$  shifts for complexes containing  $\text{B}^+$ ,  $\text{Mg}^+$ ,  $\text{Al}^+$ , and  $\text{Mn}^+$  can be linked to hybridization of the valence s orbital on the metal cation with a low-lying  $p_z$  orbital directed toward the hydrogen molecule facilitating charge transfer from the  $\text{H}_2$   $\sigma_g$  bonding orbital to a metal-centered sp hybrid orbital, thereby weakening the H–H bond.<sup>27</sup>

#### 4. Concluding Remarks

In summary, the rotationally resolved IR spectrum of  $\text{Mn}^+-\text{H}_2$  has been obtained in the H–H stretch region using photodissociation spectroscopy. Properties extracted from the spectrum include the vibrationally averaged intermolecular bond length ( $R_0 = 2.73 \text{ \AA}$ ), the H–H stretch frequency red shift ( $\Delta\nu_{\text{HH}} = -111.8 \text{ cm}^{-1}$ ), and an estimate for the harmonic intermolecular stretch frequency ( $\omega_s = 203 \text{ cm}^{-1}$ ). These data, together with the previously determined  $\text{H}_2$  binding energy ( $D_0 = 660 \text{ cm}^{-1}$ ),<sup>22</sup> establish  $\text{Mn}^+-\text{H}_2$  as a robust benchmark for calibrating ab initio and DFT calculations on systems involving open d-shell configurations and weak physisorption interactions. Ultimately, a proper theoretical description of the  $\text{Mn}^+-\text{H}_2$  complex and full comparison with the spectroscopic data will require calculation of a 3D potential energy surface, followed by rovibrational energy level calculations. This approach, as accomplished recently for  $\text{Na}^+-\text{H}_2$  and  $\text{Al}^+-\text{H}_2$ ,<sup>28,30</sup> allows direct comparisons between the calculated and measured transition energies and provides a critical test of the computed interaction potential energy surface.

**Acknowledgment.** We are grateful to the Australian Research Council and the University of Melbourne for supporting this research.

**Supporting Information Available:** Transition wavenumbers and assignments along with the full citation for ref 31.

This material is available free of charge via the Internet at <http://pubs.acs.org>.

## References and Notes

- (1) Schlapbach, L.; Zuttel, A. *Nature* **2001**, *414*, 353–358.
- (2) van den Berg, A. W. C.; Otero Areán, C. *Chem. Commun.* **2008**, 668–681.
- (3) Zhao, Y. F.; Kim, Y. H.; Dillon, A. C.; Heben, M. J.; Zhang, S. B. *Phys. Rev. Lett.* **2005**, *94*, 155504.
- (4) Yildirim, T.; Ciraci, S. *Phys. Rev. Lett.* **2005**, *94*, 175501.
- (5) Sun, O.; Wang, Q.; Jena, P.; Kawazoe, Y. *J. Am. Chem. Soc.* **2005**, *127*, 14582–14583.
- (6) Durgun, E.; Ciraci, S.; Yildirim, T. *Phys. Rev. B* **2008**, *77*, 085405.
- (7) Kim, G.; Jhi, S. H.; Park, N.; Louie, S. G.; Cohen, M. L. *Phys. Rev. B* **2008**, *78*, 085408.
- (8) Dinca, M.; Long, J. R. *Angew. Chem., Int. Ed.* **2008**, *47*, 6766–6779.
- (9) Prestipino, C.; Regli, L.; Vitillo, J. G.; Bonino, F.; Damin, A.; Lamberti, C.; Zecchina, A.; Solari, P. L.; Kongshaug, K. O.; Bordiga, S. *Chem. Mater.* **2006**, *18*, 1337–1346.
- (10) Vitillo, J. G.; Regli, L.; Chavan, S.; Ricchiardi, G.; Spoto, G.; Dietzel, P. D. C.; Bordiga, S.; Zecchina, A. *J. Am. Chem. Soc.* **2008**, *130*, 8386–8396.
- (11) Peterson, V. K.; Liu, Y.; Brown, C. M.; Kepert, C. J. *J. Am. Chem. Soc.* **2006**, *128*, 15578–15579.
- (12) Dinca, M.; Dailly, A.; Liu, Y.; Brown, C. M.; Neumann, D. A.; Long, J. R. *J. Am. Chem. Soc.* **2006**, *128*, 16876–16883.
- (13) Liu, Y.; Kabbour, H.; Brown, C. M.; Neumann, D. A.; Ahn, C. C. *Langmuir* **2008**, *24*, 4772–4777.
- (14) Duncan, M. A. *Int. Rev. Phys. Chem.* **2003**, *22*, 407–435.
- (15) MacAleese, L.; Maitre, P. *Mass Spectrom. Rev.* **2007**, *26*, 583–605.
- (16) Yang, Q. Y.; Zhong, C. L. *J. Phys. Chem. B* **2006**, *110*, 655–658.
- (17) Sun, Y. Y.; Kim, Y. H.; Zhang, S. B. *J. Am. Chem. Soc.* **2007**, *129*, 12606–12607.
- (18) Zhou, W.; Yildirim, T. *J. Phys. Chem. C* **2008**, *112*, 8132–8135.
- (19) Weinert, M.; Watson, R. E.; Fernando, G. W. *Phys. Rev. A* **2002**, *66*, 032508.
- (20) Wu, X.; Vargas, M. C.; Nayak, S.; Lotrich, V.; Scoles, G. *J. Chem. Phys.* **2001**, *115*, 8748–8757.
- (21) Kemper, P. R.; Weis, P.; Bowers, M. T.; Maitre, P. *J. Am. Chem. Soc.* **1998**, *120*, 13494–13502.
- (22) Weis, P.; Kemper, P. R.; Bowers, M. T. *J. Phys. Chem. A* **1997**, *101*, 2809–2816.
- (23) Moore, C. E. *Atomic Energy Levels As Derived from the Analyses of Optical Spectra*; U.S. National Bureau of Standards: Washington, DC, 1971; Vol. 35.
- (24) Kemper, P. R.; Weis, P.; Bowers, M. T. *Int. J. Mass Spectrom. Ion Processes* **1997**, *160*, 17–37.
- (25) Thompson, C.; Emmeluth, C.; Poad, B.; Weddle, G.; Bieske, E. *J. Chem. Phys.* **2006**, *125*, 044310–044315.
- (26) Emmeluth, C.; Poad, B. L. J.; Thompson, C. D.; Weddle, G. H.; Bieske, E. J. *J. Chem. Phys.* **2007**, *126*, 204309.
- (27) Dryza, V.; Poad, B. L. J.; Bieske, E. J. *J. Am. Chem. Soc.* **2008**, *130*, 12986–12991.
- (28) Poad, B. L. J.; Wearne, P. J.; Bieske, E. J.; Buchachenko, A. A.; Bennett, D. I. G.; Klos, J.; Alexander, M. H. *J. Chem. Phys.* **2008**, *129*, 184306–184308.
- (29) Dryza, V.; Poad, B. L.; Bieske, E. J. *J. Phys. Chem. A* **2009**, *113*, 199–204.
- (30) Emmeluth, C.; Poad, B. L. J.; Thompson, C. D.; Weddle, G. H.; Bieske, E. J.; Buchachenko, A. A.; Grinev, T. A.; Klos, J. *J. Chem. Phys.* **2007**, *127*, 164310.
- (31) Frisch, M. J.; et al. *Gaussian 03*, revision D.01; 2005. The full reference is given in the Supporting Information.
- (32) Lovejoy, C.; Nelson, D.; Nesbitt, D. J. *J. Chem. Phys.* **1987**, *87*, 5621–5628.
- (33) Bragg, S. L.; Brault, J. W.; Smith, W. H. *Astrophys. J.* **1982**, *263*, 999–1004.
- (34) Hunt, J. L.; Poll, J. D.; Wolniewicz, L. *Can. J. Phys.* **1984**, *62*, 1719–1723.
- (35) Nesbitt, D. J.; Naaman, R. *J. Chem. Phys.* **1989**, *91*, 3801.
- (36) Kemper, P. R.; Bushnell, J. E.; Weis, P.; Bowers, M. T. *J. Am. Chem. Soc.* **1998**, *120*, 7577.
- (37) Bushnell, J. E.; Kemper, P. R.; Bowers, M. T. *J. Phys. Chem.* **1994**, *98*, 2044–2049.
- (38) Kemper, P. R.; Bushnell, J.; Bowers, M. T.; Gellene, G. I. *J. Phys. Chem.* **1998**, *102*, 8590–8597.
- (39) Kraemer, W. P.; Spirko, V. *Chem. Phys.* **2006**, *330*, 190–203.
- (40) Bauschlicher, C. W. *Chem. Phys. Lett.* **1993**, *201*, 11–14.
- (41) Olkhov, R. V.; Nizkorodov, S. A.; Dopfer, O. *J. Chem. Phys.* **1997**, *107*, 8229–8238.
- (42) Vitillo, J. G.; Damin, A.; Zecchina, A.; Ricchiardi, G. *J. Chem. Phys.* **2005**, *122*, 114311/1–114311/10.

JP9031767